CHEMISTRY
A EUROPEAN JOURNAL

DOI: 10.1002/chem.200600488

# Computational Modeling of Polyoxotungstates by Relativistic DFT Calculations of $^{183}$W NMR Chemical Shifts

**Alessandro Bagno,*[a] Marcella Bonchio,[b] and Jochen Autschbach[c]**

**Abstract:** The $^{183}$W nuclear shielding in a variety of tungsten polyoxometalates (POM) (Lindqvist, Anderson, decatungstates, Keggin) of different shapes and charges has been modeled by DFT calculations that take into account relativistic effects, by means of the zero-order regular approximation (ZORA), and solvent effects, by the conductor-like screening model (COSMO) continuum method. The charge/surface area ratio ($q/A$) is proposed as an indicator of the charge density to which the solvation energies of all POMs are correlated in a satisfactory way. Among the various theoretical levels tested (ZORA scalar or spin-orbit, frozen-core or all-electron basis set, geometry optimization in the gas phase or in the continuum solvent, etc.), the best results are obtained when both geometry optimization in solvent and spin-orbit shielding are included (mean absolute error of $\delta = 35$ ppm). The quality of the computed chemical shifts depends systematically on the charge density as expressed by $q/A$; thus, POMs with low $q/A$ ratios display the best agreement with experimental data. The performance of the method is such that computed values can aid the assignment of the $^{183}$W NMR spectra of polyoxotungstates, as shown by the case of α-$[PW_{11}TiO_{40}]^{5-}$, whose six signals are ranked computationally so as to almost reproduce the experimental ordering even though the signals are spaced by as little as 5 ppm.

**Keywords:** chemical shifts · density functional calculations · NMR spectroscopy · polyoxometalates · tungsten

## Introduction

Polyoxometalates (POM) have the general formula $[X_xM_mO_y]^{q-}$, in which X is typically a main-group element and M is usually molybdenum or tungsten, and their discrete oligo-oxide structures are often considered as molecular fragments of solid metal oxide materials. POM diversity can be generated through multiple synthetic strategies that may lead to partial substitution of molybdenum or tungsten with other transition metals or functionalization with organic or organometallic groups so that a formidable variety of structures is readily accessible.[1–3]

Moreover, by taking advantage of their polyanionic nature, POM solubility can be tuned simply by choice of the countercation so that aqueous, as well as organic or alternative media, including fluorous phases, are eligible solvents.[4] For these reasons, the solution chemistry of POMs is constantly receiving increasing attention within scientific areas as diverse as homogeneous catalysis, materials science and medicinal chemistry.[2,3]

NMR analysis of the $^{183}$W nucleus ($I = {}^1/_2$, 14% natural abundance) is an essential tool for the solution characterization of diamagnetic polyoxotungstates.[5,6] It provides direct information on the electronic environment of each nonequivalent tungsten atom in these complexes. In particular, multiline $^{183}$W NMR spectra of polyoxotungstates are useful probes of the POM solution state, by displaying sets of chemical shifts sensitive to structure, solvent, and counterion.[7]

However, application of $^{183}$W NMR spectroscopy is severely hampered by the very low sensitivity of this isotope ($\gamma = 1.128 \times 10^7$ rad s$^{-1}$ T$^{-1}$, corresponding to a Larmor frequency of 16.6 MHz in a 9.4-T instrument). Even though the situation is alleviated by the very high solubility of POMs in

[a] Prof. Dr. A. Bagno
Dipartimento di Scienze Chimiche, Università di Padova
via Marzolo 1, 35131 Padova (Italy)
Fax: (+39) 049-827-5239
E-mail: alessandro.bagno@unipd.it

[b] Dr. M. Bonchio
Istituto CNR per la Tecnologia delle Membrane, Sezione di Padova
via Marzolo 1, 35131 Padova (Italy)

[c] Prof. Dr. J. Autschbach
Department of Chemistry, State University of New York at Buffalo
312 Natural Sciences Complex, Buffalo, NY 14260-3000 (USA)

Supporting information for this article is available on the WWW under http://www.chemeurj.org/ or from the author.


WILEY InterScience DISCOVER SOMETHING GREAT
© 2006 Wiley-VCH Verlag GmbH & Co. KGaA, Weinheim

water or organic solvents, attainable by selecting an appropriate countercation, recording a $^{183}W$ NMR spectrum with a good signal-to-noise ratio ($S/N$) still requires a considerable effort. There are also many instances in which high sensitivity cannot be achieved at all, for example, because the lines are broadened by scalar coupling to a quadrupolar nucleus (like $^{51}V$) or because of the presence of paramagnetic centers in reduced POMs.

Further information can often be obtained by the analysis of satellite peaks arising from scalar coupling across two bonds in each W–O–W unit.[8] The occurrence and magnitude of these $^{2}J_{WW}$ coupling constants depend on the symmetry of the POM cage and show distinctive trends according to the W–O–W angle and distances, and hence they can be usefully exploited in the assignment of spectra, although exceptions are known.[9] Indeed, empirical criteria based on relative satellite intensities have been proposed for this purpose.[10] However, satellite peaks (having 7% intensity of the main signals) are discernible only in favorable circumstances. As a consequence, the application of typical 2D NMR techniques like 2D COSY or INADEQUATE is only rarely possible;[8] 1D equivalents with selective excitation[11] only partly alleviate the problem.

Thus, under suboptimal conditions, as is often the case, one is left with just a series of singlets, possibly with the relative intensity as the only other source of information. Whereas the spectra of simple POMs can often be understood just on this basis, this may not be the case for POMs with low symmetry exhibiting between 6 and 11 individual spectral lines (but potentially many more in the case of larger POMs, for example, those belonging to the Dawson–Wells or Preyssler series).[1] There is, therefore, a genuine need for tools that may enable NMR spectroscopists to assign such spectra, even under unfavorable conditions and without recourse to empirical arguments. Moreover, it must be emphasized that a better understanding and modeling of the NMR spectra of POMs are expected to have an impact that goes beyond their structure elucidation, the aim being to develop a reliable composite tool to address both their structural and electronic properties, as well as their solution behavior.

In this respect, to take full advantage of the ability of NMR spectroscopy to detect minute differences in the electronic structures of different systems, quantum mechanical calculations represent a powerful supplementary tool. Tremendous advances have been made in this field,[12,13] so that nowadays it is possible to make meaningful predictions of the main NMR properties (chemical shift and coupling constants) of many NMR-active nuclei, which can be used for spectral assignment.

Calculations involving heavy elements have somewhat lagged behind in development owing to the notorious difficulties in handling such large systems and associated relativistic effects. Nevertheless, recent years have seen rapid progress in the field of computational NMR of heavy-atom nuclei.[13–15] Dealing with NMR properties has proved particularly demanding. The use of effective core potential basis sets is not applicable with the available (usually nonrelativistic) NMR programs for molecules since an accurate treatment of the electron density in the vicinity of the nucleus is required. So far, the implementation of efficient density-functional theory codes incorporating relativistic corrections by means of the zero-order regular approximation (ZORA)[16–22] has made this goal reachable for nuclei as heavy as $^{99}Ru$,[23] $^{103}Rh$,[24] $^{119}Sn$,[25] $^{129}Xe$,[26,27] $^{183}W$,[7,9] $^{195}Pt$, $^{199}Hg$, $^{205}Tl$, and $^{207}Pb$[14,15,28,29] (to name but a few for which sufficient data is available).

The ZORA is by no means the only available relativistic method. However, to our knowledge, so far it has been the only one for which NMR parameters have been implemented consistently with analytical-derivative techniques in the framework of DFT that includes both scalar relativistic effects and spin-orbit coupling. Furthermore, it has been shown that the approximate character of the ZORA is unlikely to be a significant source of error when calculating chemical shifts and coupling constants.[30]

A major difficulty arises in the $^{183}W$ NMR spectroscopy of polyoxotungstates. In most of the cases cited above, the accuracy of the computed values was evaluated across a chemical-shift range that may easily exceed several thousand ppm. Since most such compounds contain only one heavy atom, the accuracy is almost always sufficient to sort out such distant signals. In contrast, tungsten atoms in POMs generally lie in very similar environments ($WO_6$ octahedra), and accordingly their chemical shifts span only a small fraction of the known 8000 ppm range and tend to be very close to one another; signals separated by 1–2 ppm are not uncommon. This situation calls for significantly more stringent requirements on computational NMR methods than what is usually regarded as "satisfactory". It is the objective of this paper to show the level of accuracy that can be attained so as to set forth valuable applications for the assignment and prediction of NMR spectra. Thus, we have carried out state-of-the-art relativistic DFT calculations on a set of POMs, aiming at modeling their tungsten chemical shifts. The task is further complicated by the need to model solvent effects because POMs are negatively charged and a marked effect of the counterion and solvation has indeed been documented in several cases.[8,31,32] Quite clearly, this situation represents a major challenge for the computational approach.

In this work we calculated the tungsten nuclear shielding for a variety of POM structures. Previous work on metal chemical shifts other than those of the heaviest NMR nuclei (e.g., W, Pt, Pb, Tl) highlighted the fact that the inclusion of relativistic effects, both scalar and spin-orbit, may entail small or even negligible improvements in the calculated chemical shifts because the latter are always determined by difference.[7,15,23,25,26,28] In fact, we have previously pointed out that differences in spin-orbit shieldings may amount to a few ppm and hence provide a small but non-negligible contribution.[7] In the present instance, this cancellation of effects becomes questionable because 1) small differences are being sought and 2) for 5d elements relativistic effects influence the chemical bonds of the metal, and therefore relativ-

 © 2006 Wiley-VCH Verlag GmbH & Co. KGaA, Weinheim 

istic effects on nuclear magnetic shielding do not always originate only from core contributions that are transferable between different molecules. Nevertheless, since spin-orbit calculations are much more expensive than scalar ones, it is beneficial to investigate the accuracy at several levels of theory.

In this framework, we recall that we previously examined a small series of POM chemical shifts by ZORA scalar methods with frozen-core basis sets, obtaining a fairly good correlation with experiment, and pointed out counterion effects for lacunary POMs.[7] However, some shortcomings were also apparent, like the spread of data along two correlation lines according to the POM family, seemingly indicating an effect of overall charge. Similar findings were recently reported by Poblet and Kazansky and their co-workers.[33,34] All these observations consistently illustrate that solvation effects and the level of relativistic treatment play an important role. It was the purpose of this work to show how these problems can be overcome.

For the above reasons, this paper is organized as follows. First, a number of tests were performed in order to assess the effect of basis set and exchange-correlation functional on computed geometries and associated chemical shifts. Secondly, solvation energies were calculated in order to provide a criterion by which to classify POMs according to their charge density. Thirdly, NMR chemical shifts were calculated at the relativistic scalar and spin-orbit levels for 1) isolated ions, 2) ions in a continuum solvent model for water with the gas-phase geometry, and 3) ions in "continuum water" with the water-phase geometry. Two main parameters have been identified for use as guidelines to assess the reliability of the computational protocol with respect to experimental values, namely, 1) the mean absolute error (MAE) concerning the whole set of data and 2) the calculated spectrum of $[W_7O_{24}]^{6-}$, which consists of three well separated $^{183}W$ NMR signals. In all cases, the adherence of calculations to the experimental benchmarks will be evaluated, also with regard to the charge density parameter. The potential of our approach will finally be proved by the calculation of the NMR spectrum of $\alpha$-$[PW_{11}TiO_{40}]^{5-}$, a transition-metal-substituted polyoxotungstate. This complex displays a spin system with six nonequivalent, closely spaced $^{183}W$ signals, thus showing the level of accuracy that can be attained in a case drawn from experimental practice and of particular interest within the field of homogeneous catalysis.[35,36]

## Computational Details

All calculations were carried out using density functional theory (DFT) as implemented in the Amsterdam density functional (ADF) code[16] in which frozen-core (FC) as well as all-electron (AE) Slater basis sets are available for all atoms of interest. The most frequently used basis sets in this work were of double- and triple-zeta quality, singly polarized (DZP and TZP, respectively). The ADF code offers the possibility of taking relativistic effects into account by means of the two-component zero-order regular approximation (ZORA) method[20,28,37,38] that includes either only scalar effects (the ZORA equivalents of Darwin and mass-velocity) or spin-orbit coupling as well.

Partly owing to a cancellation of errors between the sample and reference shieldings, in the few cases studied all available GGA functionals yielded similar chemical shifts.[25,26] Nevertheless, since we are interested in comparatively small chemical shift differences, we undertook a preliminary examination of this issue. On the basis of these tests (see the Results section), we mostly adopted the Becke 88 exchange plus the Perdew 86 correlation (BP) functional.[39]

The size of the species investigated places severe limitations on the quality of the basis set that can practically be used in order to examine a representative range of POMs. In a previous work,[7] we showed that geometry optimization can be efficiently performed using the ZORA scalar method in conjunction with its specially optimized basis sets[16] using a locally dense, all-electron TZP basis set for heavy elements and the smaller double-zeta polarized DZP basis set for all other atoms. In this work we pursued the same approach, employing the all-electron TZP basis set for tungsten, tellurium, vanadium, and titanium, and the DZP basis set for germanium, phosphorus, silicon, oxygen, and boron (denoted the AE basis set for short). Note that the smaller DZP basis set was also used for the central heteroatom of $\alpha$-Keggin POMs. The geometries were then optimized taking full advantage of symmetry at the ZORA scalar level. Spin-orbit calculations were carried out on the corresponding scalar relativistic geometries.

The ADF NMR property module allows for the calculation of nuclear shieldings; details about theory and implementation are described in refs. [16,17]. Nuclear shieldings were then calculated using the scalar and spin-orbit ZORA method (ZSC and ZSO, respectively, for short) with the ZSC geometry using the AE basis set. The ZSC calculations were based on a modified version of the NMR code developed by Wolff et al.[20] in which better scaling algorithms were implemented in order to be able to treat large molecules such as the ones studied here.[27] In the ZSC case the isotropic shielding constant $\sigma$ is given by the sum of the dia- and paramagnetic contributions ($\sigma=\sigma_d+\sigma_p$), whereas in the second case the spin-orbit contribution is also added ($\sigma=\sigma_d+\sigma_p+\sigma_{SO}$). For ZORA spin-orbit calculations, the perturbed Kohn–Sham orbitals were determined at the ZORA level and included spin-orbit coupling operators (U1K BEST option in ADF).[16,20] Computed chemical shifts could then be determined by the difference between the shielding of the molecules of interest and a reference standard (for which $\delta=0$ ppm) as $\delta=\sigma_{ref}-\sigma$. Even though the accepted standard of experimental $^{183}W$ NMR spectroscopy is aqueous $WO_4^{2-}$, for reasons which will be discussed later we will mostly report chemical shifts with reference to $[W_6O_{19}]^{2-}$, which resonates at $\delta=58.6$ ppm with respect to $WO_4^{2-}$. It needs to be emphasized that although the absolute agreement between theory and experiment may be less satisfactory than one would like it to be, in many cases it is still possible to perform meaningful computational studies on a series of related compounds if the trends are correctly reproduced. This is the case here; for the purpose of studying the trends in the chemical shifts, choosing one of the POMs as the NMR reference is therefore a reasonable approach.

The corresponding shielding calculations are much more demanding than geometry optimization; this applies especially to spin-orbit calculations which currently cannot make use of molecular symmetry. While we have run a comprehensive set of all-electron calculations on POMs containing up to 12 tungsten atoms, one may wonder whether a wide range of even larger POMs, often having more than 30 tungsten atoms (like, for example, the Preyssler anion), is at all tractable by this approach. Thus, we have tested an alternative method in which the same geometry is input into a shielding calculation utilizing a smaller, less flexible frozen-core basis set: TZP (W.4f, Te.4d, V.3p) or DZP (Ge.3p, Si.2p, P.2p, B.1s, O.1s), where the notation indicates the atom and the last shell belonging to the core (for example, the 4f shell for tungsten). This basis set will be denoted as FC for short (we recall that, strictly speaking, this basis set is all-electron too, except that the orbitals designated as atomic cores are not optimized in the SCF procedure).

The solvent effect was modeled by means of the ADF implementation[40] of the COSMO method.[41] This method requires prior definition of

 © 2006 Wiley-VCH Verlag GmbH & Co. KGaA, Weinheim 

atomic radii, which were set (in Å) either at their recommended values (O: 1.7784; P: 2.106; Si: 2.457; Te: 2.4102)[16,42] or estimated (W: 2.0; V: 1.8; Ge: 1.96; B: 2.0); the radii of boron, phosphorus, silicon, and germanium are clearly not critical since they are located inside the POM cavity.

In addition to the dielectric permittivity $\varepsilon$, the solvent was also modeled by empirical parametrization of nonelectrostatic solvation terms derived from the solvation energies of alkanes.[40,43] Since these parameters are currently available only for water, energies and gradients (i.e., geometries) can be reliably calculated only for this solvent.[44] On the other hand, NMR properties are not affected by the value of these parameters. Thus, we preliminarily assessed the relevance of this problem by computing the shielding of $WO_4^{2-}$ and $[W_6O_{19}]^{2-}$ (ZSO/AE method) in other continuum solvents ranging from $CHCl_3$ ($\varepsilon=4.9$) to *N*-methylacetamide ($\varepsilon=179$) for both the gas-phase- and water-phase-optimized geometries (taken to represent geometries in nonpolar and polar solvents, respectively). Calculated shieldings level off for $\varepsilon>46.7$ (DMSO), as expected from the functional form of the reaction field in which the dielectric permittivity enters as $(\varepsilon-1)/(\varepsilon+{}^1/_2)$.[41] The observed changes did not exceed 0.7 ppm, that is, they can be considered negligible for the purposes of this work. Therefore, all subsequent calculations assumed water as the solvent, even though in several cases experimental chemical shifts were recorded in nonaqueous polar solvents. Nuclear shieldings were calculated for both the gas-phase and the COSMO (water-phase) geometries.

## Results

For this study we selected several POMs belonging to various structural groups: Lindqvist ($[W_6O_{19}]^{2-}$, $[VW_5O_{19}]^{3-}$, $[V_2W_4O_{19}]^{4-}$), Anderson ($[W_7O_{24}]^{6-}$, $[TeW_6O_{24}]^{6-}$), α-Keggin ($[BW_{12}O_{40}]^{5-}$, $[PW_{12}O_{40}]^{3-}$, $[SiW_{12}O_{40}]^{4-}$, $[GeW_{12}O_{40}]^{4-}$), and decatungstates ($[W_{10}O_{32}]^{4-}$, $[W_{10}O_{32}]^{6-}$). The selection was made so as to have a set of spectra 1) spanning a wide range of chemical shifts (ca. 500 ppm) while still lying in a relatively narrow range of POMs and 2) whose assignment is unquestionable, either because it can be readily made on the basis of symmetry and relative intensities or because a single signal is present.

The selected POMs also do not possess vacant sites, which are known to entail specific counterion and solvent effects.[31,32] These effects require a separate study, which is currently in progress. We note, in particular, that the series of Keggin POMs, α-$[XW_{12}O_{40}]^{n-}$, differing only in the central heteroatom (X = B, Si, P, Ge), and the $[W_{10}O_{32}]^{4-/6-}$ redox pair, allow the charge effect on $^{183}W$ chemical shifts in an isostructural series to be evaluated.

After extensive testing as detailed below, eight combinations of method, basis set, and treatment of solvent were investigated: 1) ZSC/FC, 2) ZSO/FC, 3) ZSC/AE, 4) ZSC/AE with COSMO, gas-phase geometry, 5) ZSC/AE with COSMO, water geometry, and 6–8) the ZSO/AE calculations corresponding to points (3)–(5). The polyanions investigated are given in Table 1 with the experimental conditions and chemical shifts and are depicted in Figure 1. Each

Table 1. Experimental data, literature sources, and calculated $^{183}W$ chemical shifts [ppm] of polyoxotungstates.[a]

| POM, symmetry[b] | Abbrev. | Exptl[c] | | Counterion/Solvent | FC | | | ZSC/AE | | | ZSO/AE | |
|---|---|---|---|---|---|---|---|---|---|---|---|---|
| | | Rel. $WO_4^{2-}$ | Rel. W6 | | ZSC | ZSO | Gas phase | COSMO (gas geom.) | COSMO (water geom.) | Gas phase | COSMO (gas geom.) | COSMO (water geom.) |
| $[W_6O_{19}]^{2-}$, $O_h$ | W6 | 58.9 | 0 | $Bu_4N$/(MeCN/DMF)[d] | 0 | 0 | 0 | 0 | 0 | 0 | 0 | 0 |
| $[VW_5O_{19}]^{3-}$, $C_{4v}$ (ax) | VW5 | 75.9 | 17 | $Bu_4N$/MeCN[e] | 38.8 | 22.2 | 26.7 | 68.0 | 33.7 | 39.5 | 42.9 | 2.9 |
| $[VW_5O_{19}]^{3-}$ (eq) | | 76.4 | 17.5 | | 13.9 | 41.5 | 63.0 | 30.7 | −7.7 | 65.6 | 69.8 | 33.8 |
| $[V_2W_4O_{19}]^{4-}$, $C_s$ | V2W4 | 70.3 | 11.4 | $Li/H_2O$[e] | 65.5 | 34.4 | 92.6 | 100.0 | 47.2 | 103.3 | 111.4 | 56.8 |
| $[V_2W_4O_{19}]^{4-}$ | | 69.4 | 10.5 | | 19.6 | 66.5 | 48.9 | 54.8 | 2.0 | 71.2 | 77.6 | 22.8 |
| $[W_{10}O_{32}]^{4-}$, $D_{4h}$ (ax) | W10 | −165.6 | −224.5 | $Bu_4N$/MeCN[f] | −270.0 | −261.2 | −286.1 | −282.3 | −306.7 | −291.0 | −285.9 | −310.9 |
| $[W_{10}O_{32}]^{4-}$ (eq) | | −22.5 | −81.4 | | −115.1 | −67.7 | −113.9 | −115.3 | −135.5 | −43.2 | −44.2 | −64.4 |
| $[W_{10}O_{32}]^{6-}$, $D_{4h}$ (ax) | W10red | −149 | −207.9 | $Bu_4N$/MeCN[f] | −174.8 | −179.6 | −167.3 | −156.0 | −265.3 | −191.9 | −176.7 | −288.9 |
| $[W_{10}O_{32}]^{6-}$ (eq) | | 307 | 248.1 | | 142.1 | 194.8 | 215.2 | 213.0 | 126.6 | 288.4 | 289.2 | 201.6 |
| $[W_7O_{24}]^{6-}$, $C_{2v}$ (4) | W7 | −91.8 | −150.7 | $Na/H_2O$[g] | −64.1 | 1.4 | −75.4 | −73.4 | −209.4 | 11.2 | 15.4 | −139.6 |
| $[W_7O_{24}]^{6-}$ (2) | | −178.9 | −237.8 | | −70.5 | −30.6 | −61.3 | −67.9 | −205.0 | −9.3 | −12.0 | −160.0 |
| $[W_7O_{24}]^{6-}$ (1) | | 269.2 | 210.3 | | 89.0 | 144.0 | 115.9 | 123.8 | 71.4 | 200.7 | 208.0 | 151.5 |
| $[TeW_6O_{24}]^{6-}$, $D_{3d}$ | TeW6 | −115.8 | −174.7 | imidazolium/$H_2O$[h] | −89.2 | −39.9 | −126.9 | −120.6 | −205.2 | −63.8 | −54.4 | −155.0 |
| α-$[BW_{12}O_{40}]^{5-}$, $T_d$ | BW12 | −130.8 | −189.7 | $H/H_2O$[i] | −256.4 | −203.4 | −249.7 | −246.8 | −252.2 | −174.6 | −170.0 | −169.9 |
| α-$[PW_{12}O_{40}]^{3-}$, $T_d$ | PW12 | −99 | −157.9 | $H/H_2O$[i] | −270.4 | −209.4 | −269.1 | −270.2 | −272.6 | −185.6 | −187.0 | −188.7 |
| α-$[SiW_{12}O_{40}]^{4-}$, $T_d$ | SiW12 | −103.8 | −162.7 | $H/H_2O$[i] | −226.8 | −168.6 | −218.2 | −217.1 | −217.1 | −139.6 | −138.0 | −137.8 |
| α-$[GeW_{12}O_{40}]^{4-}$, $T_d$ | GeW12 | −81.9 | −140.8 | $H/H_2O$[i] | −194.5 | −137.5 | −183.4 | −182.5 | −182.5 | −107.0 | −105.4 | −105.3 |
| MAE[j] | | | | | 63 | 51 | 59 | 60 | 55 | 58 | 61 | 35 |
| slope[k] | | | | | 0.78 | 0.76 | 0.90 | 0.90 | 0.92 | 0.91 | 0.91 | 0.93 |
| intercept[k] | | | | | −24 | 8.0 | −5.7 | −2.7 | −51 | 40 | 44 | −7.0 |

[a] See the text and Tables S1–S8 for details. [b] Where applicable, the assignment and relative intensity are given in parentheses; ax and eq labels denote axial and equatorial tungsten atoms, respectively. [c] Chemical shifts relative to 2 M $Na_2WO_4$ or to the value for $[W_6O_{19}]^{2-}$ ($\delta=58.9$ ppm). [d] See ref. [45]. [e] See ref. [46]. Not assigned, but can be considered essentially equal. [f] See ref. [47]. [g] See ref. [48]. [h] See ref. [49]. [i] See ref. [50]. [j] Mean absolute error in chemical shifts relative to $[W_6O_{19}]^{2-}$. [k] Fit parameters of $\delta_{calcd}=a\delta_{exptl}+b$.


© 2006 Wiley-VCH Verlag GmbH & Co. KGaA, Weinheim

complete data set (including individual contributions to $\sigma$) is collected in the Supporting Information (Tables S1–S8 and associated plots).

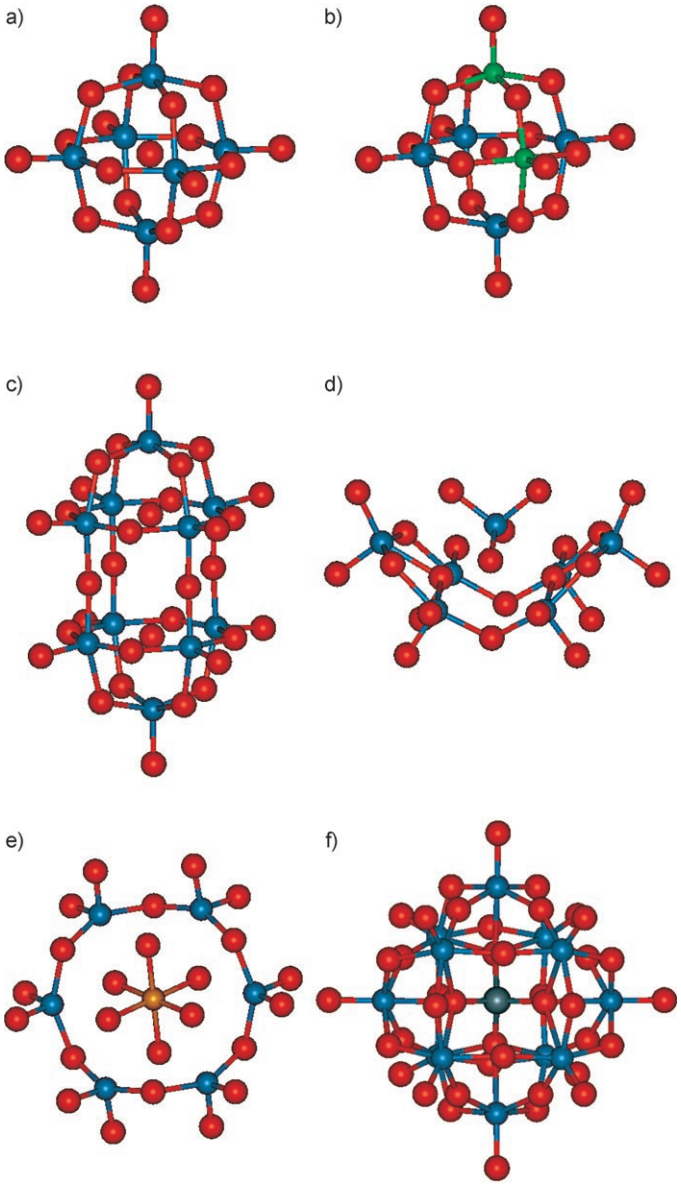


Figure 1. Representative structures of the polyoxometalates investigated in this work (BP-ZORA scalar/AE). a) $[W_6O_{19}]^{2-}$; b) $[V_2W_4O_{19}]^{4-}$ (the structure of $[VW_5O_{19}]^{3-}$ is the same, with only one vanadium atom); c) $[W_{10}O_{32}]^{4-/6-}$; d) $[W_7O_{24}]^{6-}$; e) $[TeW_6O_{24}]^{6-}$; f) $[XW_{12}O_{40}]^{n-}$ (X = B, Si, P, Ge). W: blue; O: red; V: green; Te: orange; X: grey. Structures optimized at other levels (e.g., in the COSMO continuum solvent) are visually indistinguishable. See the Supporting Information for Cartesian coordinates.

**General remarks**: Note that the basic building block of the POMs, that is, monomeric $WO_4^{2-}$, does not fit well in the correlations. Whereas this may be somewhat expected (tungstate is not a polyoxometalate), this feature highlights some general limitations of the computational approach. Since the departure from POM trends, occurring at all levels, becomes even more important when solvent effects are taken into account (see below), it appears more sensible to refer all data to that of a POM for which no ambiguity exists, like $[W_6O_{19}]^{2-}$. For this reason, we will evaluate the general performance of the various theoretical levels by comparing the values of the mean absolute error in the chemical shifts referenced in this way. Note also the spectrum of $[W_7O_{24}]^{6-}$, which features three signals in a 4:2:1 ratio, and hence is independently assignable. The performance of the various methods will often be evaluated on the basis of the correlation of this single spectrum (i.e., whether the ordering of these signals is correct).

**XC functional and basis-set effects on gas-phase geometries**: The structures of the POMs feature at least two types of W–O bonds, namely terminal bonds ($WO_t$) with double-bond character and bridging bonds ($WO_b$) with single-bond character. Some POMs also feature a central, hexacoordinated oxygen atom ($O_c$) (see Figure 1). In this test and those that follow, no solvent effect was included.

We first tested the performance of a few GGA functionals by optimizing the geometry of $WO_4^{2-}$ and $[W_6O_{19}]^{2-}$ with the BP,[39] PW91,[51] PBE,[52] and BLYP[53] functionals (ZSC/TZP level). The first three functionals led to very similar geometries (to within 0.001 Å), whereas the BLYP functional led to slightly shorter distances, slightly improving (by 0.01 Å) the agreement with experiment. Given its marginally better performance, and also in view of the performance with respect to NMR properties (see below), we preliminarily selected the BP functional. This had the additional advantage of being consistent with other related computational work on POMs.[7,9,33,34,54–58]

In order to assess the performance of the locally dense AE basis set we are advocating, we tested the performance of a few larger basis sets, namely a uniform basis on all atoms: 1) TZP, 2) TZ2P, and 3) QZ4P (see ref. [16] for definitions). These tests were run on a representative subset of the POMs investigated, that is, 1) on W6, W10, TeW6, W7, and PW12 and 2) and 3) on $WO_4^{2-}$ and W6 only.

In the gas phase (isolated ion) at the BP-ZORA scalar/AE level, all POMs investigated have average $WO_t$ and $WO_b$ bond lengths of 1.76 and 1.96 Å, respectively. In the parent $WO_4^{2-}$ ion the $WO_t$ bond (1.816 Å) is longer than the POM average. Increasing the basis set, as in 1), leads to small changes, mostly negative ($\Delta r = -0.02$ to $+0.001$ Å), in the W–O bond lengths of all POMs. The higher levels, 1) and 2), lead to a further shortening of the W–O bonds by −0.001 Å each. It is then apparent that the geometries are already essentially converged with the AE basis set.

The experimentally determined WO bond length in $WO_4^{2-}$ (1.7–1.8 Å)[59] compares fairly well with the calculated one (1.816 Å), which is overestimated by 0.1 Å. Similar trends are apparent for all the other POMs: for $[W_6O_{19}]^{2-}$, $[PW_{12}O_{40}]^{3-}$, $[SiW_{12}O_{40}]^{4-}$,[1] $[W_{10}O_{32}]^{4-}$,[60] $[W_7O_{24}]^{6-}$,[61] and $[TeW_6O_{24}]^{6-}$,[49] the $WO_t$ bonds are overestimated by 0.01–0.05 Å. Most $WO_b$ bonds are also overestimated (by 0.02–

 © 2006 Wiley-VCH Verlag GmbH & Co. KGaA, Weinheim 

0.05 Å), except those of Keggin POMs, which are underestimated by 0.5 Å.

Thus, the general performance of the computational method can be judged to be only fair, as previously noted.[62] In any event, there does not seem to be an easy solution to this problem: as seen above, the performance of larger basis sets is not substantially better (although the trend is in the right direction).

**XC functional and basis-set effects on nuclear shieldings**: Further tests concerned the quality of the calculated shieldings of the above subset of POMs with various combinations of XC functional and basis set, particularly in comparison with the locally dense AE basis set (TZP-DZP) or the TZP basis set on all atoms. Thus, after geometry optimization chemical shifts were calculated at the same level of theory. In order to avoid misleading results, the tests were performed at the highest available level (ZSO with ZSC geometries).

We first probed the relative performance of the BP and BLYP functionals, which had previously been found to lead to somewhat different geometries. This test was run on $WO_4^{2-}$, W6, TeW6, and W7 (TZP basis set). The MAEs of the chemical shifts calculated with the BP and BLYP functionals were 119 and 129 ppm, respectively. Thus, we feel confident in using the BP functional from hereafter.

The final tests concerned the performance of the AE (TZP-DZP), TZP, TZ2P, and QZ4P basis sets on W6, W10, TeW6, and W7. For this data subset, the MAE with the AE basis set was 88 ppm. By adopting a uniform TZP basis set, the chemical shift of $[W_6O_{19}]^{2-}$ with respect to $WO_4^{2-}$ was improved (161 vs. 74 ppm; exptl 58.9 ppm), but the quality of the overall correlation became worse, with a MAE of 101 ppm. Further tests concerned only the chemical shift of $[W_6O_{19}]^{2-}$: the larger TZ2P and QZ4P basis sets gave values of $\delta = 49$ and $-82$ ppm, respectively. Thus, while TZ2P gives the smallest difference, QZ4P did not perform particularly well and its high computational cost also needs to be considered. Similar findings regarding the QZ4P basis set were previously reported for $^{199}$Hg chemical shift tensors.[63]

Note that some of the basis set truncation might in fact compensate for deficiencies in the calculated geometries and the neglect of explicit solvation effects. A recent study of $^{195}$Pt chemical shifts has indicated that reasonable agreement with experiment can be obtained at the ZORA/COSMO/TZP level because of a compensation of errors; a source of error may be the neglect of nonspecific solvent effects.[64] The molecular dynamics approach with a highly flexible basis set in a comparatively large explicit solvation shell would clearly be preferable, but this would require averaging of 50–100 chemical shifts calculated at the spin-orbit ZORA level along the dynamics trajectory, and for the POMs studied here this is clearly not feasible in the near future. It is possible that the findings for $^{195}$Pt chemical shifts are transferable to the POM case here, which underlines again the issue of absolute versus relative accuracy of the NMR calculations.

Summarizing, the BP/TZP-DZP level of theory offers a good balance of performance and cost, and we will further proceed on these grounds.

**Geometries in water**: The geometries of all the POMs investigated, optimized in the gas phase and in water (as modeled by COSMO), show noticeable systematic differences. All bond lengths shorten upon hydration ($\Delta r = -0.009$, $-0.003$, and $-0.005$ Å for $WO_t$, $WO_b$, and $WO_c$, respectively). One can measure the overall variation by monitoring the "edge-to-edge" distance ($r_{ee}$), that is, the distance between the two farthest terminal oxygen atoms, which gives an estimate of the overall size of the POM. Thus, $\Delta r_{ee}$ is negative ($\Delta r_{ee} = -0.074$ Å on average, that is, ca. 1%) and POMs contract upon hydration.[62] Even these rather small changes are more than sufficient to cause marked changes in the calculated tungsten shieldings, which affect the general performance of the calculation, as detailed below. It is worthwhile recalling at this point that the uniform TZP basis set leads to geometry changes that are qualitatively the same as those caused by solvation. However, since this basis set does not provide consistently better chemical shifts, it is apparent that the different geometry alone cannot account for the different performances of the solvation methods.

**Solvation energies**: Poblet and co-workers have investigated several issues related to the solvation of POMs, that is, the electronic structure of POMs in relation to their charge/mass ratio,[54–57] the solvent effect on the stability of variously reduced POMs,[58] as well as the average location of the solvent and counterions in the vicinity of a POM by means of molecular dynamics simulations in water.[65]

COSMO calculations allow the energies of ionic solvation to be estimated, together with its dissection into electrostatic and nonelectrostatic (cavitation, dispersion) terms (Table 2). All the POMs investigated feature a small and fairly constant nonelectrostatic solvation energy of around 2–3 kcal mol$^{-1}$, which slightly increases with ionic size as expected. By far, of course, the main term is the electrostatic one,

Table 2. Calculated solvation energies and charge densities of POMs.

| POM | $E_{solv}$ (el)[a,b] | $E_{solv}$ (ne)[a,c] | $E_{solv}$[a] | $q/m$[d] | $10^2\ q/A$[e] |
|---|---|---|---|---|---|
| $[WO_4]^{2-}$ | −215.7 | 1.82 | −213.9 | 2.00 | 0.719 |
| $[W_6O_{19}]^{2-}$ | −142.2 | 2.39 | −139.8 | 0.33 | 0.346 |
| $[VW_5O_{19}]^{3-}$ | −311.3 | 2.38 | −308.9 | 0.50 | 0.523 |
| $[V_2W_4O_{19}]^{4-}$ | −546.0 | 2.36 | −543.6 | 0.67 | 0.706 |
| $[W_{10}O_{32}]^{4-}$ | −462.3 | 2.77 | −459.6 | 0.40 | 0.509 |
| $[W_{10}O_{32}]^{6-}$ | −1025 | 2.78 | −1022 | 0.60 | 0.758 |
| $[W_7O_{24}]^{6-}$ | −1103 | 2.57 | −1100 | 0.86 | 0.884 |
| $[TeW_6O_{24}]^{6-}$ | −1098 | 2.60 | −1096 | 1.00 | 0.869 |
| α-$[BW_{12}O_{40}]^{5-}$ | −675.7 | 2.96 | −672.7 | 0.42 | 0.564 |
| α-$[PW_{12}O_{40}]^{3-}$ | −246.9 | 2.97 | −243.9 | 0.25 | 0.336 |
| α-$[SiW_{12}O_{40}]^{4-}$ | −433.9 | 2.97 | −430.9 | 0.33 | 0.448 |
| α-$[GeW_{12}O_{40}]^{4-}$ | −433.4 | 2.98 | −430.4 | 0.33 | 0.447 |

[a] In kcal mol$^{-1}$ from COSMO calculation on the water-phase geometry. [b] Electrostatic term. [c] Non-electrostatic terms (cavitation and dispersion). [d] Ratio of total charge and number of metal atoms (W or V) in the main POM framework. [e] Ratio of total charge and surface area [Å$^2$] as computed by the COSMO method.

 © 2006 Wiley-VCH Verlag GmbH & Co. KGaA, Weinheim 

ranging from $-215.7$ kcal mol$^{-1}$ for $[W_6O_{19}]^{2-}$ to $-1103$ kcal mol$^{-1}$ for $[W_7O_{24}]^{6-}$. Following Poblet and co-workers' approach, which links charge distribution and associated solvation properties to the $q/m$ ratio,[54–57] that is, to the ratio between the overall charge and the number of metal (tungsten or other) atoms in the main POM framework, we have correlated these two parameters in Figure 2a. Indeed, the solvation energies and charge densities are correlated, albeit with a noticeable scatter. Labeling the data points according to the parent structure highlights a different dependence of Lindqvist- and Keggin-type POMs, each family displaying a good correlation with $q/m$. Similar results are obtained if the charge/volume ratio ($q/V$ or VCD) is used, as recently proposed by Poblet and co-workers.[66] In particular, the charge effect on otherwise similar POMs like the Keggin $\alpha$-$[XW_{12}O_{40}]^{n-}$ is apparent, the least exothermic solvation being calculated for X=P ($n=3$), the most exothermic for X=B ($n=5$), and identical intermediate values for the tetra-anions with X=Si and Ge. The effect is even more evident in the $[W_{10}O_{32}]^{4-/6-}$ pair, whose solvation energies vary by a factor of 2.2 as an effect of the change in total charge (and fit fairly well with the Keggin-type data). Conversely, $WO_4^{2-}$ has a rather low solvation energy ($-213.9$ kcal mol$^{-1}$) despite the highest $q/m$ value, which highlights its entirely different electronic structure and response to solvent.

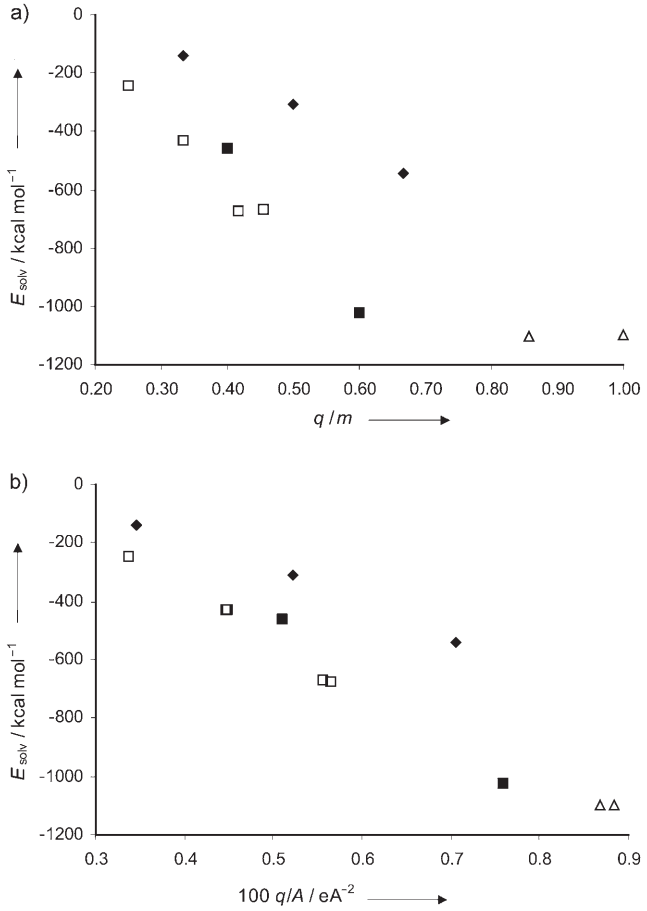


Figure 2. Correlation between calculated solvation energies and a) the charge/mass ratio $q/m$ and b) the charge/surface area ratio $q/A$ for POMs. Filled squares: W10 and W10red; empty squares: $\alpha$-Keggin; diamonds: Lindqvist; triangles: W7 and TeW6. The data point for $WO_4^{2-}$ has been omitted.

This approach assumes a relationship between the number of metal atoms and the overall size of the species. This relationship can be expected to hold only if all species share the same shape. Whereas most POMs indeed share an approximately spherical shape, some do not, notably, the Anderson POMs investigated here. This may have a bearing on the way $m$ is determined; the X heteroatom in $\alpha$-$[XW_{12}O_{40}]^{n-}$ is not included in $q/m$ because it is completely screened from the environment, but in the case of $[TeW_6O_{24}]^{6-}$ the tellurium atom is in fact quite exposed (Figure 1) and its inclusion in $q/m$ is purely subjective. Thus, Figure 2a shows that $[TeW_6O_{24}]^{6-}$ and $[W_7O_{24}]^{6-}$ have very similar solvation energies despite rather different $q/m$ values. Since the interaction with solvent takes place through the accessible surface area, it makes sense to adopt an alternative measure of charge density, for instance the ratio of charge to surface area (as calculated by the COSMO procedure). These results are presented in Figure 2b and show a generally better correlation, even though the data for Lindqvist POMs still seem to define a slightly different trend.

**Calculations with frozen-core basis sets**: All the results are collected in Table 1. With regard to those obtained with frozen-core basis sets on gas-phase structures, while a general trend is apparent, a large degree of scattering is present. Indeed, the mean absolute error (MAE) of $\delta=63$ ppm at the scalar level only allows for the assignment of chemical-shift ranges, rather than of individual resonances. A considerable improvement is attained when spin-orbit effects are included: the MAE drops to $\delta=51$ ppm ($\sigma_{SO}$ values span a sizable 71 ppm range, as previously noted[7]). In either case, the assignment of $[W_{10}O_{32}]^{4-}$, $[W_{10}O_{32}]^{6-}$, and $[W_7O_{24}]^{6-}$ would be feasible without difficulty. For $[W_7O_{24}]^{6-}$, at the SO level, an excellent linearity is obtained ($r^2=0.999$) for the three signals, even though the slope of this limited correlation is only 0.4.

**Calculations with all-electron basis sets—the ZORA scalar method**: For $[BW_{12}O_{40}]^{5-}$, $[SiW_{12}O_{40}]^{4-}$, and $[GeW_{12}O_{40}]^{4-}$, the COSMO optimization did not lead to any structural change and identical shieldings have been used in the pertinent correlations. Conversely, for $[PW_{12}O_{40}]^{3-}$, geometry optimization led to a slightly different structure. For gas-phase structures, one does not notice major improvements (Table 1) compared with the much less expensive frozen-core method. Indeed, the MAE remains fairly high (59–60 ppm) for both the gas-phase and COSMO calculations. Going to COSMO-optimized structures only leads to a slight improvement (MAE=55 ppm).

 © 2006 Wiley-VCH Verlag GmbH & Co. KGaA, Weinheim 

**Calculations with all-electron basis sets—the ZORA spin-orbit method**: The results obtained with the spin-orbit ZORA method and all-electron basis sets, with and without solvent effects, are also collected in Table 1. The results for the isolated ions are of the same quality as those from the scalar calculations, with a MAE of 58 ppm. Parallel to the scalar results, the results obtained using the COSMO method with gas-phase geometries led to a similar outcome (MAE = 61 ppm).

In contrast, a major improvement is observed only when the solvent effects are included in both geometry optimization and NMR calculations. This is the highest level approach adopted here and yields a MAE of only 35 ppm (about half of the other values) across a 500 ppm range embracing POMs of widely varying structure, charge, and $q/m$ (or $q/A$) ratio. Moreover, the correlation line (relative to $[W_6O_{19}]^{2-}$) has a slope closest to unity (0.93), an almost zero intercept (−7 ppm), and a correlation coefficient of 0.905 (Figure 3). The ordering and spacings of the signals of $[W_7O_{24}]^{6-}$ are again correct, with a slope of 0.73.

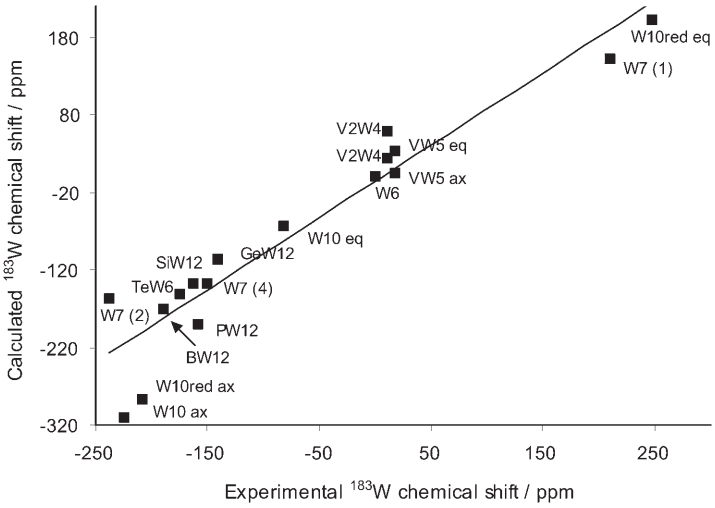


Figure 3. Correlation between calculated and experimental $^{183}$W chemical shifts in polyoxometalates relative to $[W_6O_{19}]^{2-}$. ZORA spin-orbit, all-electron basis set; COSMO calculations at the COSMO-optimized geometry in water. The correlation line has a slope of 0.93, an intercept of −7 ppm, and $r^2 = 0.905$.

The overall trends in the signed and absolute errors as a function of theoretical level and POM charge are sketched in Figure 4.

**Assignment of the spectrum of α-$[PW_{11}TiO_{40}]^{5-}$**: Up to this point, we have shown that the most accurate level investigated (ZORA spin-orbit with COSMO-optimized geometry) provides a mean average error of $\delta = 35$ ppm. Thus, as expected, the spectrum of $[W_7O_{24}]^{6-}$ is easily assignable on this basis, since its three signals are separated by at least 87 ppm. However, this situation is by no means a common one: in typical cases, peak separations are much smaller, and often smaller than the lowest MAE we have obtained. The question then naturally arises as to whether this computational protocol can have any applicability in typical NMR practice. In the following, we will address this issue by showing that the attainable accuracy can in fact be higher.

To this end, we will consider the $^{183}$W NMR spectrum of α-$[PW_{11}TiO_{40}]^{5-}$. As a monosubstituted α-Keggin derivative, it has $C_s$ symmetry and hence displays six nonequivalent tungsten environments, corresponding to six individual NMR peaks; its structure and numbering are given in Figure 5. The tungsten atom lying on the symmetry plane (W6) gives rise to a signal of half intensity, so the six signals have a ratio of 2:2:2:2:2:1 and W6 is the only one that can be unambiguously assigned.[8] In this POM the signals span 60 ppm, with peak separations as small as 2–5 ppm; the spectrum has been assigned by means of the usual criteria based on the magnitude of the $^2J_{WW}$ couplings.[67] Even though the assignment appears to be quite sound, we have previously shown that such criteria are not always reliable.[9] The experimental and calculated chemical shifts are collected in Table 3 and plotted in Figure 6; since W6 can be identified with confidence, we compare the shifts with this signal. Experimentally, one finds the signals in the order W1 > W5 > W6 > W3 > W4 > W2.

We have run two series of calculations at the ZORA spin-orbit level with the AE basis set: in the gas phase and in water with COSMO-optimized geometry. In view of the previous results and of the high computational expense we did not carry out a COSMO calculation on the gas-phase geometry. Geometry optimization in the continuum solvent causes a shrinkage of the overall size of the POM cage by 0.7%, that is, similar to that of the other POMs.

The chemical shifts calculated in the gas phase give a fairly good correlation with a MAE of 10 ppm, but the order is W1 > W5 > W3 > W6 > W2 > W4. Conversely, the calculation that allows for solvation effects not only yields a smaller MAE (6 ppm), but the ordering is W1 > W5 > W3 > W6 > W4 > W2, that is, only W3 and W6 (for which $\Delta\delta = 5$–7 ppm) are interchanged. Thus, the trend previously identified is also found to hold in this case. We note in particular that use of the COSMO method results in large changes in the shifts of W1 and W4, that is, the tungsten nuclei closest to the titanium atom. We also note that its charge density and solvation energy ($q/A = 5.57 \times 10^{-3}\, e\,\text{Å}^{-2}$; $E_{solv} = -669$ kcal mol$^{-1}$) fit perfectly the trend defined by the other Keggin POMs of Figure 2b. These results are best appreciated by looking at the stick spectra of Figure 7.

## Discussion

The correlation in Figure 3 spans a 500 ppm region in which most POM $^{183}$W NMR resonances are observed. Even though this region is substantially narrower than the whole $^{183}$W NMR range of 8000 ppm, a remarkable correlation is found with calculated values, which holds for a wide variety of structural and charge types.

 © 2006 Wiley-VCH Verlag GmbH & Co. KGaA, Weinheim 

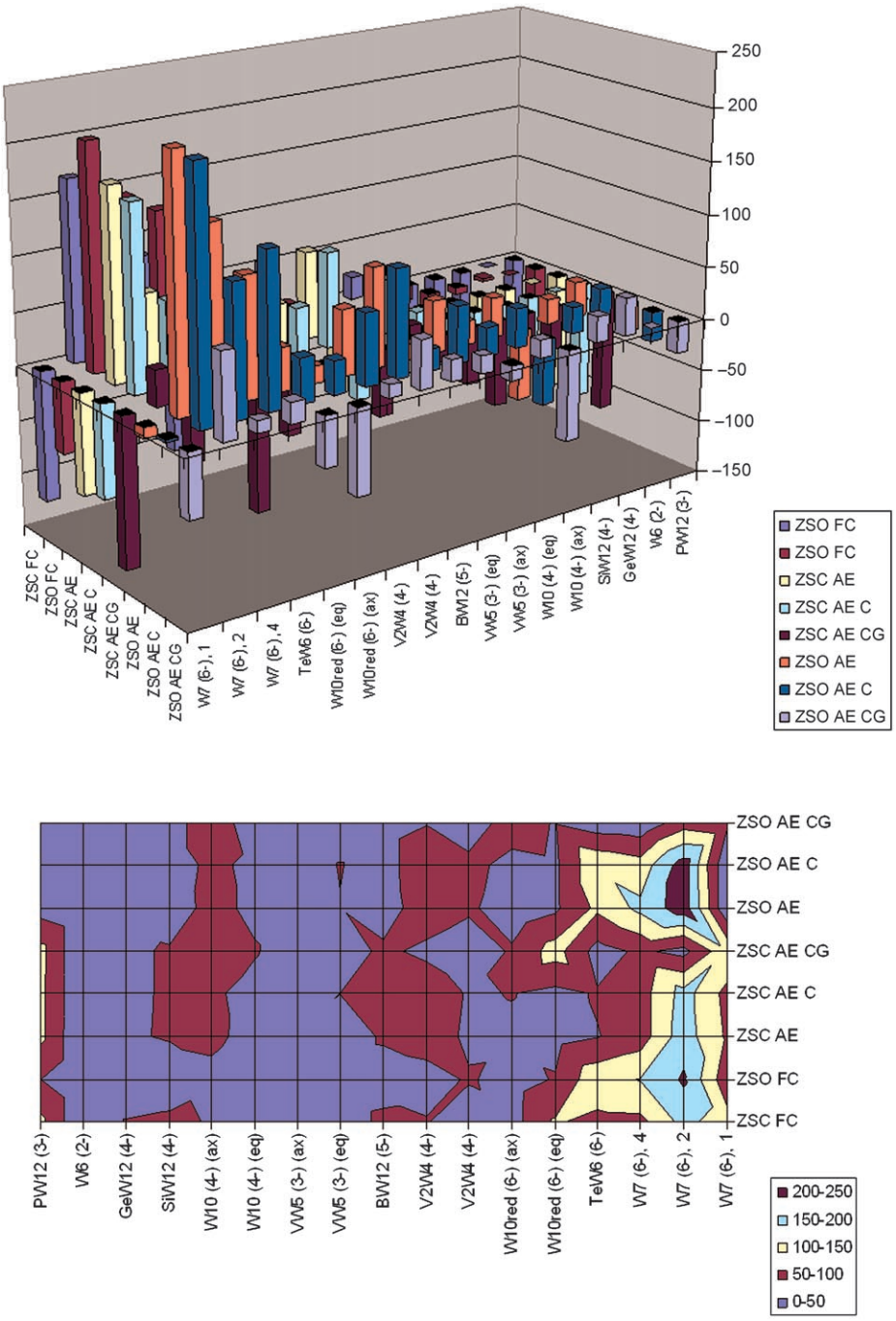


Figure 4. Errors in the chemical shifts of the POMs as a function of theoretical level (arranged according to increasing computational size) and $q/A$ (see text). Top: 3D histogram with signed errors. Bottom: Color map with unsigned errors. C: COSMO, gas-phase geometry; CG: COSMO, water-phase geometry.

However, even by considering only the results obtained at the ZORA spin-orbit level with COSMO-optimized geometries (Figure 2), one cannot fail to notice the scatter in the correlation, which remains lower in quality than those already presented for many other NMR-active nuclei, especially light ones. In this respect, it should be noted that POMs present substantial complications relative to most other nuclei that have been studied computationally.

First, the experimental data are not homogeneous, since they span countercations from $H^+$ to $Bu_4N^+$ and were recorded in different solvents. The large variability in experimental conditions can be easily traced to the difficulty in recording $^{183}W$ NMR spectra, which calls for the highest possible concentrations and hampers the collection of a homogeneous data set. Some allowance must then be made for the variability in the experimental data.

Secondly, the influence of solvent cannot be overemphasized: indeed, one can hardly expect a continuum solvent model such as COSMO (or its equivalents) to model all the complex and long-range interactions taking place in concentrated electrolyte solutions such as those typically employed in $^{183}W$ NMR studies. The solvation shell (and dynamics thereof) of these ionic species can be probed by molecular dynamics simulations,[65] and these calculations will eventually furnish valuable data on the local solute–solvent arrangement in solution. Indeed, a fully dynamic structure in solution is expected to yield a vast improvement in computed spectroscopic properties; however, this approach[68,69] is not yet feasible for systems of this size.

Thirdly, the counterion effect has been neglected except for indirect effects that might be incorporated in the COSMO solvent model through the net charge of the solvation surface. Even though the explicit inclusion of small ions like $Na^+$ would not burden the calculations too much, given the almost spherical structure and smooth charge distribution of POMs any placement of one or more counterions in the vicinity of the anion would be arbitrary and not representative of the average situation in solution in the absence of other information. (This would not hold for lacunary POMs, which, however, are beyond the scope of this paper.)

 © 2006 Wiley-VCH Verlag GmbH & Co. KGaA, Weinheim 

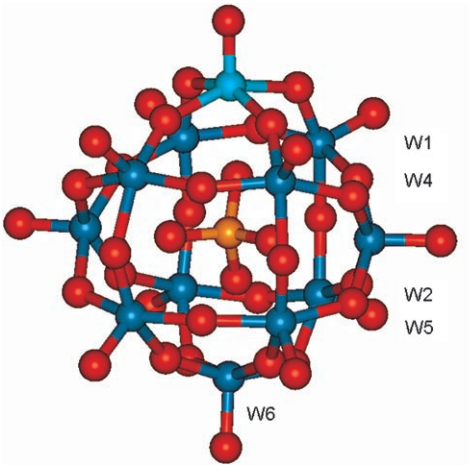


Figure 5. Structure and numbering of α-$[PW_{11}TiO_{40}]^{5-}$ (BP-ZORA scalar/AE). W: blue; O: red; P: orange; Ti: cyan. See the Supporting Information for Cartesian coordinates.

Table 3. Experimental and calculated $^{183}$W chemical shifts [ppm] of α-$[PW_{11}TiO_{40}]^{5-}$.[a]

| | Exptl | | Gas phase | COSMO |
|---|---|---|---|---|
| | Rel. $WO_4^{2-}$ | Rel. W6 | Rel. W6 | |
| W1 | −57.2 | 44.7 | 24.8 | 39.8 |
| W2 | −118 | −16.1 | −10.6 | −9.3 |
| W3 | −106.7 | −4.8 | 6.9 | 4.4 |
| W4 | −109.2 | −7.3 | −17.0 | −3.2 |
| W5 | −92.6 | 9.3 | 14.2 | 12.7 |
| W6 | −101.9 | 0 | 0 | 0 |
| MAE[b] | | | 10 | 6 |

[a] Experimental data for the $Bu_4N$ salt in MeCN from ref. [67]. Calculations at the BP-ZORA spin-orbit AE level. [b] Average error in the chemical shifts of W1–W5.

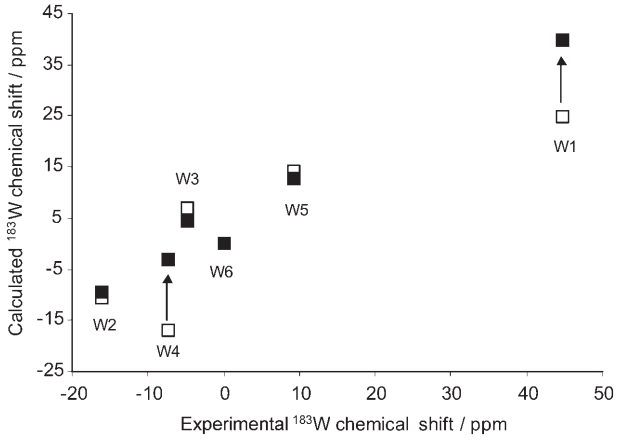


Figure 6. Correlation between the calculated and experimental $^{183}$W chemical shifts of α-$[PW_{11}TiO_{40}]^{5-}$ relative to the unique W6 signal (ZORA spin-orbit, AE basis set). Empty squares: gas-phase calculations (MAE = 10 ppm); filled squares: COSMO calculations on the COSMO-optimized geometry in water (MAE = 6 ppm). The arrows highlight the large changes to the shielding of W1 and W4 caused by solvation.

In this respect, there is a recognizable relationship between the signed error of the chemical shift of each POM and its $q/A$ or $q/m$ ratio, which holds at all theoretical levels. This is shown in Figure 4; it is evident that the largest deviations occur, essentially at all theoretical levels, for POMs having a high $q/A$ (or $q/m$) ratio (leftmost region of the histogram in Figure 4, top). Likewise, the foremost row (ZSO with COSMO on COSMO-optimized geometry) illustrates at a glance the consistently better performance of this method even in difficult cases. The color map of Figure 4, bottom, provides an alternative overview in which it is clearly seen that 1) the left region (POMs with low charge density) is characterized by smaller absolute errors than the right region and 2) upon going from bottom to top (i.e., improving the theoretical level) mean absolute errors decrease.

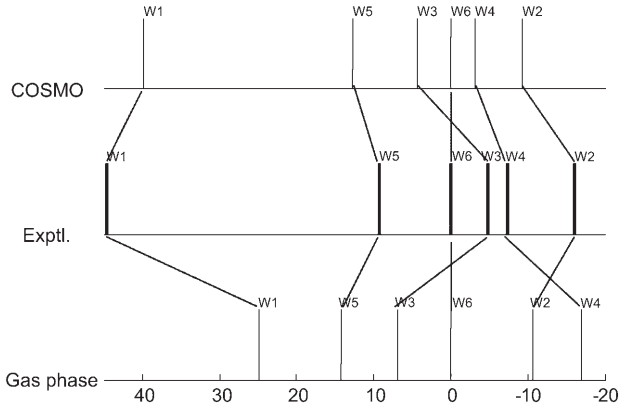


Figure 7. Stick $^{183}$W NMR spectra of α-$[PW_{11}TiO_{40}]^{5-}$ relative to the W6 signal. Top to bottom: COSMO calculation in water; experimental; gas-phase calculation.

It is also very reassuring that the best overall agreement with experiment is obtained with our highest-level computational model. In this connection, one should note that the fairly good performance of frozen-core calculations (whose MAE is comparable to or even smaller than that of all-electron scalar calculations, see Table 1) is probably due to a cancellation of errors. Nevertheless, this approach might be useful to establish at least some general trends, for example in the case of very large POMs.

In general, the inclusion of solvent effects through the COSMO method leads to a consistently better performance than for the corresponding gas-phase calculations. More importantly, the best performance is obtained when the solvent also exerts its effect in the geometry optimization. Thus, coupling the small (ca. 1%) structural shrinkage upon solvation with the solvent effect on the shielding provides a noticeably better agreement with experiment.

It is then evident that the chemical shifts of $^{183}$W in POMs are affected by solvent effects. From our results we conclude that most of these effects can be handled by a continuum method unless the charge density is relatively large. In such cases, inclusion of the solvent is absolutely essential to reach any meaningful conclusion and the quality of the predictions remains somewhat worse.

In turn, these findings highlight some features of the solvation of POMs that need to be further investigated. For ex-

 © 2006 Wiley-VCH Verlag GmbH & Co. KGaA, Weinheim 

ample, the shape of the POM seems to play an important role. The solvation energies of W7 and TeW6 are anomalous if related to that of the more common, spherically shaped POMs, whereas they fit into a general trend if one takes their flattened shape into account. Thus, in TeW6 the solvation of the central $TeO_6$ unit should probably be considered, whereas the solvation of the central, inner $XO_4$ unit in Keggin POMs has an effect only indirectly by altering the overall geometry.

Summarizing, relativistic DFT calculations that include solvation effects provide remarkable accuracy in computed chemical shifts. Even so, one may raise a legitimate question as to whether an average error of 35 ppm, however remarkable, is at all useful in common NMR practice. We have seen that the three widely spaced signals of W7 can be assigned without difficulty; nevertheless, the range encompassed by most POMs is much narrower. We have tried to address this issue by considering a more "typical" POM-like $\alpha$-$[PW_{11}TiO_{40}]^{5-}$. Remarkably, these calculations seem to indicate that the attainable accuracy is substantially better when the analysis is limited to different signals of the same species; the MAE of 6 ppm is such that most differences in chemical shift may be resolved computationally, thus providing proof of the concept for the computational protocol. While these results need to be confirmed with a greater variety of examples, there is a good prospect that this approach can be applied to the amazing structural variety of POMs. In any event, the composite solvent effect on both geometry and shieldings is borne out also in this case.

Finally note that the computational effort required for this type of calculation escalates rapidly with the number of tungsten atoms, so that larger or less symmetric POMs (for which several more chemical shifts would have to be computed) may hardly be tractable, except in highly parallel computer environments. Hence, it is worthwhile exploring possible shortcuts that afford a similar accuracy. In this respect, one notes that the diamagnetic shielding ($\sigma_d$) varies very little along the whole series, 7–8 ppm by all methods (see also refs. [7,33,34]). This is expected because the electronic structure of the core shells hardly changes along a series in which the formal oxidation state remains in most cases at $W^{VI}$ ($d^0$). The calculation of the $\sigma_d$ term is quite time-consuming (because we use a nonhybrid functional there is no need for an iterative solution of the CPKS equations, which makes the $\sigma_p$ and $\sigma_d$ terms roughly equally expensive[20]). Hence, one may consider calculating only $\sigma_p$ and $\sigma_{SO}$, which, as expected, show a strong dependence on the structure (maximum ranges are 400–500 ppm for $\sigma_p$ and 100 ppm for $\sigma_{SO}$). The availability of each individual contribution allows this possibility to be evaluated: indeed, neglecting the large, but relatively constant, $\sigma_d$ term (details in Table S8 of the Supplementary Information) leads to a correlation line whose fit parameters are identical to those previously mentioned. The recognition of this may lead to a substantial speeding up of further calculations on larger POMs.

## Conclusion

We have computed $^{183}W$ NMR chemical shifts of polyoxotungstates of widely varying structures and charge densities by means of relativistic DFT methods. The performances of various combinations of method, basis set, and relativistic treatment have been evaluated. Despite the large variations considered and the inherent difficulty in modeling charged species in polar solvents, ZORA spin-orbit calculations with inclusion of solvent effects (by means of the COSMO method) have provided an average accuracy of 35 ppm, that is, about 7% of the encompassed range. We have also highlighted major solvent effects on the chemical shifts of POMs with high charge densities, as expressed as the charge/area ($q/A$) ratio. Finally, we have analyzed the six nonequivalent $^{183}W$ NMR signals of the substituted Keggin POM $\alpha$-$[PW_{11}TiO_{40}]^{5-}$ as a prototypical example of an NMR spectrum drawn from common NMR practice and found an average error of 6 ppm, which enables one to rank almost all signals in the experimentally found order. Thus, these calculations can be expected to considerably aid NMR spectroscopists in the structural assignment of POMs of unknown structure.

## Acknowledgements

This work was financially supported by the University of Padova (Progetto di Ricerca di Ateneo CPDA045589) and was carried out within the framework of COST Action D26/0015/04. J.A. acknowledges financial support from the CAREER program of the National Science Foundation (CHE-0447321) and from the ACS Petroleum Research Fund (40987-G3).

[1] M. T. Pope, *Heteropoly and Isopoly Oxometalates (Inorganic Chemistry Concepts, Vol. 8)*, Springer, Berlin, **1983**.
[2] *Polyoxometalates* (Ed.: C. L. Hill), thematic issue of *Chem. Rev.* **1998**, *98*, 1.
[3] *Polyoxometalate Chemistry for Nano-Composite Design* (Eds.: T. Yamase, M. T. Pope), Kluwer Academic, Plenum, New York, **2002**, p. 1.
[4] M. Vazylyev, D. Sloboda-Rozner, A. Haimov, G. Maayan, R. Neumann, *Top. Catal.* **2005**, *34*, 93.
[5] D. Rehder in *Multinuclear NMR* (Ed.: J. Mason), Plenum, New York, **1987**.
[6] Y.-G. Chen, J. Gong, L.-Y. Qu, *Coord. Chem. Rev.* **2004**, *248*, 245.
[7] A. Bagno, M. Bonchio, A. Sartorel, G. Scorrano, *ChemPhysChem* **2003**, *4*, 517.
[8] C. Brevard, R. Schimpf, G. Tourne, C. M. Tourne, *J. Am. Chem. Soc.* **1983**, *105*, 7059.
[9] A. Bagno, M. Bonchio, *Angew. Chem.* **2005**, *117*, 2059; *Angew. Chem. Int. Ed.* **2005**, *44*, 2023.
[10] N. N. Sveshnikov, M. T. Pope, *Inorg. Chem.* **2000**, *39*, 591.
[11] A. Bagno, M. Bonchio, A. Sartorel, G. Scorrano, *Eur. J. Inorg. Chem.* **2000**, 17.
[12] T. Helgaker, M. Jaszuński, K. Ruud, *Chem. Rev.* **1999**, *99*, 293.
[13] *Calculation of NMR and EPR Parameters* (Eds.: M. Kaupp, M. Bühl, V. G. Malkin), Wiley-VCH, Weinheim, **2004**.
[14] J. Autschbach in *Principles and Applications of Density Functional Theory in Inorganic Chemistry I, Vol. 112* (Eds.: N. Kaltsoyannis, J. E. McGrady), Springer, Heidelberg, **2004**, p. 1.

 © 2006 Wiley-VCH Verlag GmbH & Co. KGaA, Weinheim 

[15] J. Autschbach, T. Ziegler in *Encyclopedia of Nuclear Magnetic Resonance, Vol. 9* (Eds.: D. M. Grant, R. K. Harris), Wiley, Chichester, **2002**, p. 306.
[16] a) G. te Velde, F. M. Bickelhaupt, E. J. Baerends, C. Fonseca Guerra, S. J. A. van Gisbergen, J. G. Snijders, T. Ziegler, *J. Comput. Chem.* **2001**, *22*, 931; see also: b) ADF 2004.01, ADF User's Guide, http://www.scm.com, SCM, Theoretical Chemistry, Vrije Universiteit, Amsterdam
[17] E. van Lenthe, E. J. Baerends, J. G. Snijders, *J. Chem. Phys.* **1993**, *99*, 4597.
[18] E. van Lenthe, E. J. Baerends, J. G. Snijders, *J. Chem. Phys.* **1994**, *101*, 9783.
[19] E. van Lenthe, A. Ehlers, E. J. Baerends, *J. Chem. Phys.* **1999**, *110*, 8943.
[20] S. K. Wolff, T. Ziegler, E. van Lenthe, E. J. Baerends, *J. Chem. Phys.* **1999**, *110*, 7689.
[21] J. Autschbach, T. Ziegler, *J. Chem. Phys.* **2000**, *113*, 936.
[22] J. Autschbach, T. Ziegler, *J. Chem. Phys.* **2000**, *113*, 9410.
[23] A. Bagno, M. Bonchio, *Magn. Reson. Chem.* **2004**, *42*, S79.
[24] L. Orian, A. Bisello, S. Santi, A. Ceccon, G. Saielli, *Chem. Eur. J.* **2004**, *10*, 4029.
[25] A. Bagno, G. Casella, G. Saielli, *J. Chem. Theory Comput.* **2006**, *2*, 37.
[26] A. Bagno, G. Saielli, *Chem. Eur. J.* **2003**, *9*, 1486.
[27] J. Autschbach, E. Zurek, *J. Phys. Chem. A* **2003**, *107*, 4967.
[28] J. Autschbach in *Calculation of NMR and EPR Parameters* (Eds.: M. Kaupp, M. Bühl, V. G. Malkin), Wiley-VCH, Weinheim, **2004**, Chapter 14.
[29] J. Autschbach, T. Ziegler in *Calculation of NMR and EPR Parameters. Theory and Applications* (Eds.: M. Kaupp, M. Bühl, V. G. Malkin), Wiley-VCH, Weinheim, **2004**, Chapter 15.
[30] J. Autschbach, *Theor. Chem. Acc.* **2004**, *112*, 52.
[31] J. F. Kirby, L. C. W. Baker, *Inorg. Chem.* **1998**, *37*, 5537.
[32] V. A. Grigoriev, D. Cheng, C. L. Hill, I. A. Weinstock, *J. Am. Chem. Soc.* **2001**, *123*, 5292, and references therein.
[33] J. Gracia, J. M. Poblet, J. Autschbach, L. P. Kazansky, *Eur. J. Inorg. Chem.* **2006**, 1139.
[34] J. Gracia, J. M. Poblet, J. A. Fernández, J. Autschbach, L. P. Kazansky, *Eur. J. Inorg. Chem.* **2006**, 1149.
[35] O. A. Kholdeeva, T. A. Trubitsina, R. I. Maksimovskaya, A. V. Golovin, W. A. Neiwert, B. A. Kolesov, X. Lopez, J. M. Poblet, *Inorg. Chem.* **2004**, *43*, 2284.
[36] O. A. Kholdeeva, T. A. Trubitsina, G. M. Maksimov, A. V. Golovin, R. I. Maksimovskaya, *Inorg. Chem.* **2005**, *44*, 1635.
[37] E. van Lenthe, E. J. Baerends, J. G. Snijders, *J. Chem. Phys.* **1993**, *99*, 4597.
[38] E. van Lenthe, Ph.D. Thesis, Vrije Universiteit (Amsterdam), **1996**.
[39] a) A. D. Becke, *Phys. Rev. A* **1988**, *38*, 3098; b) J. P. Perdew, *Phys. Rev. B* **1986**, *33*, 8822.
[40] C. C. Pye, T. Ziegler, *Theor. Chem. Acc.* **1999**, *101*, 396.
[41] a) A. Klamt, G. Schüürmann, *J. Chem. Soc., Perkin Trans. 2* **1993**, 799; b) A. Klamt, V. Jones, *J. Chem. Phys.* **1996**, *105*, 9972; c) A. Klamt, *J. Phys. Chem.* **1995**, *99*, 2224.
[42] Recommended radii from: A. Bondi, *J. Phys. Chem.* **1964**, *68*, 441.
[43] T. N. Truong, E. V. Stefanovich, *Chem. Phys. Lett.* **1995**, *240*, 253.
[44] It is worth noting that the thermodynamics of solvation of hydrocarbons is profoundly different according to whether the solvent is water or practically any other liquid, see, for example: W. Blokzijl, J. B. F. N. Engberts, *Angew. Chem.* **1993**, *105*, 1610; *Angew. Chem. Int. Ed. Engl.* **1993**, *32*, 1545.
[45] O. A. Gansow, R. K. C. Ho, W. G. Klemperer, *J. Organomet. Chem.* **1980**, *187*, C27.
[46] P. J. Domaille, *J. Am. Chem. Soc.* **1984**, *106*, 7677.
[47] D. C. Duncan, C. L. Hill, *Inorg. Chem.* **1996**, *35*, 5828.
[48] R. I. Maksimovskaya, K. G. Burtseva, *Polyhedron* **1985**, *4*, 1559.
[49] P. A. Lorenzo-Luis, P. Gili, A. Sánchez, E. Rodriguez-Castellon, J. Jiménez-Jiménez, C. Ruiz-Pérez, X. Solans, *Transition Met. Chem.* **1999**, *24*, 686.
[50] R. Acerete, C. F. Hammer, L. C. W. Baker, *J. Am. Chem. Soc.* **1982**, *104*, 5384.
[51] J. P. Perdew, J. A. Chevary, S. H. Vosko, K. A. Jackson, M. R. Pederson, D. J. Singh, C. Fiolhais, *Phys. Rev. B* **1992**, *46*, 6671.
[52] J. P. Perdew, K. Burke, M. Ernzerhof, *Phys. Rev. Lett.* **1996**, *77*, 3865.
[53] a) A. D. Becke, *Phys. Rev. A* **1988**, *38*, 3098; b) C. Lee, W. Yang, R. G. Parr, *Phys. Rev. B* **1988**, *37*, 785; c) B. G. Johnson, P. M. W. Gill, J. A. Pople, *J. Chem. Phys.* **1993**, *98*, 5612; d) T. V. Russo, R. L. Martin, P. J. Hay, *J. Chem. Phys.* **1994**, *101*, 7729.
[54] J. M. Maestre, X. López, C. Bo, J. M. Poblet, *J. Am. Chem. Soc.* **2001**, *123*, 3749.
[55] X. López, J. M. Maestre, C. Bo, J. M. Poblet, *J. Am. Chem. Soc.* **2001**, *123*, 9571.
[56] X. López, C. Bo, J. M. Poblet, *J. Am. Chem. Soc.* **2002**, *124*, 12574.
[57] J. M. Poblet, X. López, C. Bo, *Chem. Soc. Rev.* **2003**, *32*, 297.
[58] X. López, J. M. Poblet, *Inorg. Chem.* **2004**, *43*, 6863.
[59] A. Thiele, J. Fuchs, *Z. Naturforsch.* **1979**, *34b*, 145.
[60] J. Fuchs, H. Hartl, W. Schiller, U. Gerlach, *Acta Crystallogr., Sect. B* **1976**, *32*, 740.
[61] K. Ikenoue, M. Mikuriya, O. Miyauchi, R. Nukada, B. Yagasaki, *Bull. Chem. Soc. Jpn.* **1994**, *67*, 2590.
[62] X. López, J. A. Fernández, S. Romo, J. F. Paul, L. P. Kazansky, J. M. Poblet, *J. Comput. Chem.* **2004**, *25*, 1542.
[63] J. Jokisaari, S. Jarvinen, J. Autschbach, T. Ziegler, *J. Phys. Chem. A* **2002**, *106*, 9313.
[64] a) M. Sterzel, J. Autschbach, *Inorg. Chem.*, 2006, 45, 3316; see also b) E. P. Fowe, P. Belser, C. Daul, H. Chermette, *Phys. Chem. Chem. Phys.* **2005**, *7*, 1732.
[65] X. López, C. Nieto-Draghi, C. Bo, J. Bonet Avalos, J. M. Poblet, *J. Phys. Chem. A* **2005**, *109*, 1216.
[66] X. López, J. A. Fernández, J. M. Poblet, *Dalton Trans.* **2006**, 1162.
[67] W. H. Knoth, P. J. Domaille, D. C. Roe, *Inorg. Chem.* **1983**, *22*, 198.
[68] M. Bühl, S. Grigoleit, H. Kabrede, F. T. Mauschick, *Chem. Eur. J.* **2006**, *12*, 477.
[69] M. Pavone, G. Brancato, G. Morelli, V. Barone, *ChemPhysChem* **2006**, *7*, 148.

Received: April 6, 2006
Published online: August 22, 2006

 © 2006 Wiley-VCH Verlag GmbH & Co. KGaA, Weinheim 